Compressive Failure of Notched Carbon Fibre Composites

C. Soutis; P. T. Curtis; N. A. Fleck

Proceedings: Mathematical and Physical Sciences, Vol. 440, No. 1909 (Feb. 8, 1993), 241-256.

Compressive failure of notched carbon fibre composites

By C. Soutis,[1] P. T. Curtis[2] and N. A. Fleck[3]

[1]*Leicester University Engineering Department, University Road, Leicester LE1 7RH, U.K.*

[2]*Materials and Structures Department, Defence Research Agency, Farnborough GU14 6TD, U.K.*

[3]*Cambridge University Engineering Department, Trumpington Street, Cambridge CB2 1PZ, U.K.*

We present an investigation into the compressive fracture properties of carbon fibre/epoxy laminates. Unnotched and notched strengths are reported for a wide range of 'lay-ups', and results are interpreted in terms of existing theories of strength. In all cases, we find that compressive failure is governed by plastic microbuckling of the 0° plies. For unnotched laminates, the failure strain is independent of lay-up configuration, suggesting that a critical strain to failure, or maximum strain criterion can predict the failure point adequately. In tests on notched panels, the growth of damage from the edge of a single hole is examined. For notched materials, the failure strength and damage zone size at failure support the prediction of the Soutis, Fleck and Smith model.

1. Introduction

Long fibre composites such as carbon fibres in an epoxy matrix, offer the design engineer a material of high stiffness and strength combined with low density. Composite materials are widely used in laminated sheet form in the aerospace industry and to a lesser extent in the automotive industry. They are manufactured with successive layers in differing directions in order to meet the multiaxial stress requirements of aerospace components and to maximize the effect of the poor transverse properties of unidirectional material. Typical components contain many holes, introduced either intentionally as cut-outs and as fastener holes, or unintentionally due to damage events.

The tensile strength of these materials is derived mainly from the high tensile strength of the fibres. In compression, however, the matrix and fibre–matrix interface assume important roles because they must provide lateral support for the fibres and prevent them from undergoing column buckling. While much research work has been conducted into the tensile failure of composite panels containing holes (see review by Awerbuch & Madhukar (1985)) relatively little is known about compressive failure in notched components. The main reason for this is the difficulty associated with compression testing, in particular in achieving true material failures within the gauge length of the specimen (Curtis 1991).

Early work on carbon fibre reinforced epoxy materials demonstrated that they failed in compression by fibre shear or crushing for test temperatures below 100 °C,

Proc. R. Soc. Lond. A (1993) **440**, 241–256
Printed in Great Britain

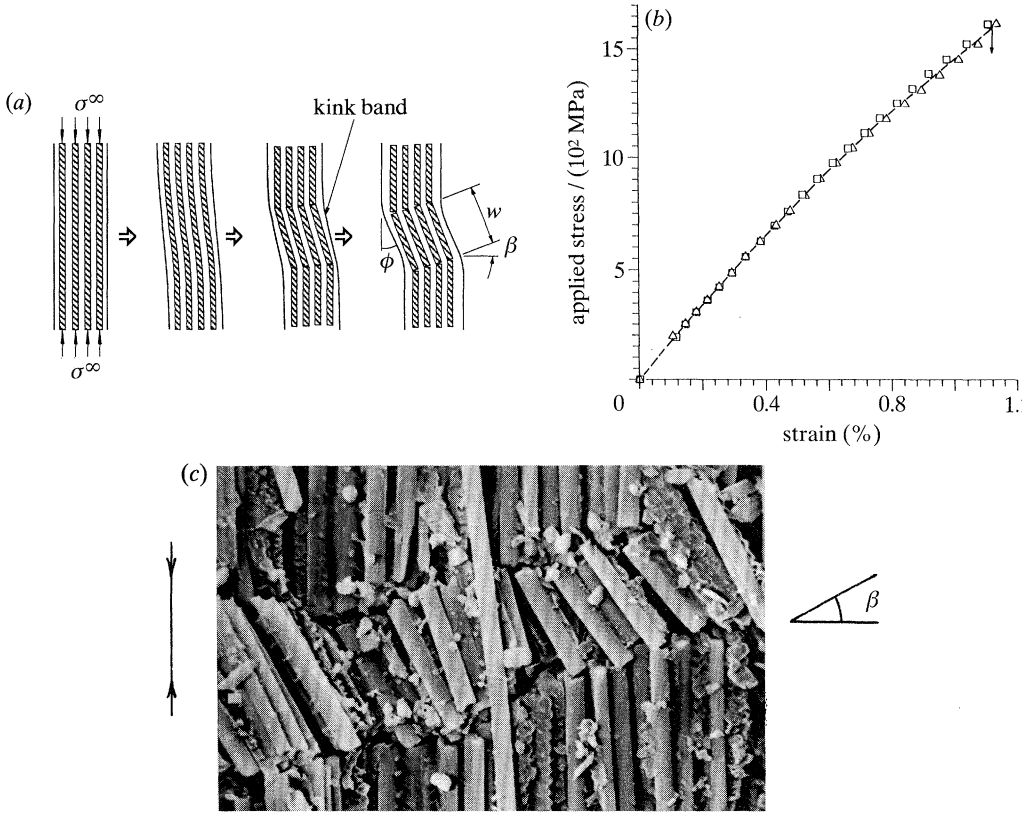

Figure 1. Geometry of fibre microbuckling mode (β is the orientation of microbuckle band, ϕ is the fibre rotation in band, w is the microbuckle width). (*b*) Stress–strain response of the unidirectional laminate. The strains on both faces are almost the same, indicating insignificant bending. ———, Average axial strain; □, strain at front face; △, strain at back face. (*c*) Scanning electron micrograph showing fibre microbuckling in a T800/924C unidirectional laminate. Two planes of fracture form creating a kink band of width $w = 50$–60 μm, and orientation $\beta = 15°$.

Ewins & Ham (1973). At higher temperatures, sufficient reduction in the matrix strength occurred, allowing fibre microbuckling to become the dominant failure mechanism, see figure 1*a*. Over the past two decades the tensile strength of carbon fibres has doubled but compressive strength has improved very little. Epoxy matrix materials have been developed with increased strength and higher ductility in an attempt to impart to the composite high toughness and impact resistance. Modern carbon fibre–epoxy composites fail in compression by microbuckling at ambient temperatures, and possess a compressive strength which is of the order of 60 % of the tensile strength.

In the present paper an experimental investigation is reported into the compressive failure processes of carbon fibre–epoxy panels. The effect of laminate ply lay-up upon unnotched and notched strength is determined, and results are compared with existing theoretical models.

Table 1. *Unnotched strength properties*

lay-up	ply-orientation	% 0° plies	σ_{un} MPa	E^c_{yy} GPa	G^d_{xy} GPa	ϵ_f (%)	K_c MPa m$^{\frac{1}{2}}$	$(K_c/\sigma_{un})^2$ mm
L0	$[0_8]_s$	100	1615	160	6	1.10	—	—
L1	$[(\pm 45/0_4)_2]_s$	67	1010 (1136)[a]	109	17.76	1.04	50.5	2.50
L2	$[(\pm 45/0_2)_3]_s$	50	810 (904)[a]	88	23.5	1.10	46.5	3.29
L3	$[(0/90_2/0)_3]_s$	50	670[b] (847)[a]	78	6.0	0.96	40.6	2.30
L4	$[\pm 45/0_2/90_2/0_2/90_2/0_2]_s$	50	820 (865)[a]	84	12.0	1.05	40.0	2.38
L5	$[(\pm 45/0/90)_3]_s$	25	568 (523)[a]	58	23.6	1.07	42.5	5.60
L6	$[(\pm 45)_2/0/(\pm 45)_2/0/\pm 45]_s$	17	428 (442)[a]	41	35.4	1.35	35.0	6.68

[a] Predicted values, assuming elastic laminate plate theory and $\epsilon_f = 1.1\,\%$.
[b] Premature failure due to out-of-plane microbuckling.
[c] E_{yy} is the laminate stiffness in the loading direction.
[d] G_{xy} is the shear stiffness obtained from the laminate plate theory.

2. Unnotched strength of T800/924C carbon–epoxy panels

Multidirectional laminates were autoclaved from Toray T800 source carbon fibres preimpregnated with Ciba-Geigy BSL 924C epoxy resin. The material was laid up by hand in 1 m × 0.3 m panels with seven different stacking sequences, as summarized in table 1. The proportion of 0° layers was varied from 100 % to 17 %. All multidirectional laminates were symmetric about the mid-plane, consisted of 24 plies and were approximately 3 mm thick. Following cure, the laminates were inspected ultrasonically to confirm specimen quality.

Compression tests were performed on unidirectional material (laminate designation L0) using a modified Celanese test rig (Curtis 1985). The specimens were end-tabbed and of gauge section 10 mm × 10 mm; this gauge length is sufficiently short for anti-buckling guides not to be required. The multidirectional specimens (laminates L1–L6, see table 1) were of gauge section 116 mm × 30 mm, and were tested by using an anti-buckling device to prevent macrobuckling during the test. Aluminium end tabs were bonded to the specimens. All tests were conducted in a screw-driven test machine at a displacement rate of 0.017 mm s^{-1}, and strain gauges were used on both faces of test pieces to measure axial strain, and to monitor the degree of bending. Full details on the experimental technique have been documented previously by Soutis (1991). At least five tests were performed for each lay-up.

(*a*) *Test results*

Typical compressive stress–strain response of the $[0_8]_s$ laminate is shown in figure 1*b*. The measured strains on the two faces indicated insignificant bending, implying that the test method successfully generated true compressive failures in the material. The stress–strain response is linear with an elastic modulus $E = 160$ GPa, up to a strain of 0.3 %. At higher strains the response is slightly nonlinear, and the tangential modulus at failure is 10 % less than that of the initial linear part. Catastrophic failure

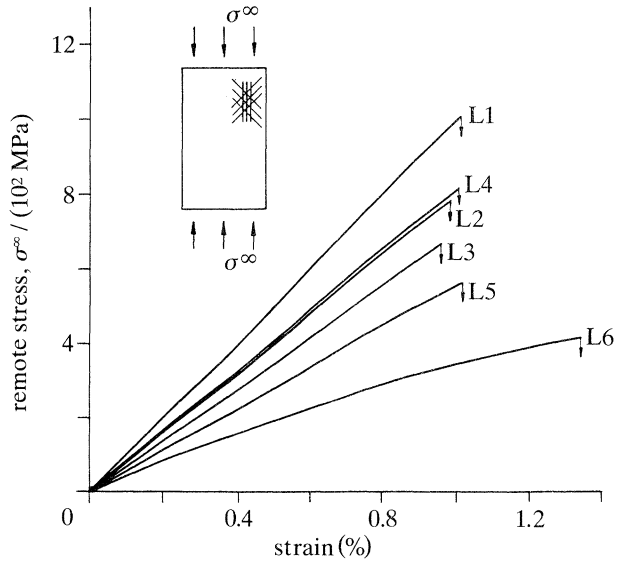

Figure 2. Uniaxial compressive stress–strain response for T800/92+C laminates L1–L6.

occurs at an average failure stress $\sigma_f = 1600$ MPa, and an average failure strain $\epsilon_f = 1.1\,\%$. In comparison, the average tensile strength for this material equals 2400 MPa. Post-failure examination of the fracture surfaces using a scanning electron microscope revealed that failure is by fibre microbuckling. The fibres break at two points, and create a kink band inclined at an angle, $\beta \approx 15°$, to the transverse direction, see figure 1*c*. The fibres within the band rotate by an angle $\phi = 30°$ from the initial fibre direction, and the kink width $w = 50$–60 μm is approximately equal to 10 fibre diameters ($d = 5.5$ μm).

In the multidirectional materials, laminates L1–L6, failure is always by microbuckling of the 0° plies, and is accompanied by delamination between the off-axis and 0° plies, and by plastic deformation in the off-axis plies. The scatter in strength is less than 10 % and the failure strain $\epsilon_f = 1\,\%$ is almost independent of lay-up and comparable to the failure strain of the unidirectional laminate, see figure 2. This suggests that the off-axis plies have little influence upon the strain for microbuckling of the 0° layers, perhaps because the 0° plies are much stiffer than the off-axis plies and carry most of the load. The critical event in these laminates is microbuckling of the 0° fibres leading to failure by the nucleation and growth of a kink band at an angle $\beta = 5$–$20°$.

It is worth noting that the failure strain of laminate L3 is less than that of L4. Laminate L3 contains 0° outer layers which fail by out-of-plane microbuckling, but laminate L4 possesses $\pm 45°$ outer plies which support the 0° inner layers permitting them to fail by in-plane microbuckling, which is a higher strain failure event. Laminate L6 is primarily composed of $\pm 45°$ plies which have low axial stiffness. This lay-up displays a nonlinear stress–strain response, and fails at a higher strain, $\epsilon_f = 1.35\,\%$, than that of the other laminates. The failure strain of L6 is, however, markedly less than the failure strain of $\epsilon_f = 6\,\%$ exhibited by laminates comprising $100\,\% \pm 45°$ material (Soutis 1991).

(*b*) *Comparison with theory*

Several theoretical models have been developed to quantify the compressive failure of unidirectional material due to microbuckling (see, for example, Rosen 1965; Argon 1972; Budiansky 1983; Steif 1990*a*, *b*). These models have been reviewed in detail recently by Soutis (1991) and Budiansky & Fleck (1991). There is strong experimental and theoretical support for the argument that microbuckling of unidirectional material is governed by the shear yield stress τ_y of an elastic-perfectly plastic composite, and the misalignment angle of the fibres $\bar{\phi}$. Budiansky (1983) has presented a kinking analysis which suggests that the compressive strength σ_{cr} is given by

$$\sigma_{cr} = \tau_y/(\bar{\phi}+\gamma_y), \tag{2.2.1}$$

where γ_y is the shear yield strain of the composite. Substitution of strength values for unidirectional T800/924C material into (2.2.1) gives $\bar{\phi} = 3.0°$, which is comparable with measured values of fibre misalignment (Yurgatis 1987).

Laminate plate theory may be used to estimate the failure strength of multidirectional laminates if it is assumed that the strain in the composite is uniform, that the response is linear elastic to failure, and that the failure strain ϵ_f equals that of unidirectional material. The predicted strength using the maximum strain criterion combine with laminate theory is within 10% of the measured strength, see table 1.

3. Review of theoretical models for compressive failure from a hole

Compressive failure from a hole in a multidirectional composite panel is by the initiation and growth of a microbuckle from the edge of the hole (Soutis & Fleck 1990). This process has been modelled with varying degrees of sophistication. Early models assumed that failure occurred when the maximum stress in the structure equals the unnotched compressive strength of the material (maximum stress criterion), or that failure occurs when the net section stress in the structure equals the unnotched compressive strength (net section stress criterion) (Peterson 1974). Nuismer & Labor (1979) applied the average stress failure criterion and Rhodes *et al.* (1984) the point stress failure criterion to predict the strength of composite panels with holes loaded in compression. The above criteria were developed by Whitney & Nuismer (1974) for notched (hole or crack) plates under uniaxial tension. They introduced a characteristic length by assuming that fracture depends on attaining a critical stress (equal to unnotched strength) at a characteristic distance d_0 ahead of the cut-out, or attaining a critical average stress along a characteristic distance a_0 ahead of the notch. The characteristic distance is used as a free parameter to be fixed by best fitting the experimental data. Guynn *et al.* (1989) compared the microbuckled zone at the edges of a hole in carbon–epoxy and carbon–PEEK laminates to an equivalent crack containing constant cohesive stresses. This analysis predicted the size of the buckled region as a function of the applied load, with the constant local stress supported by the buckled fibres being an adjustable parameter similar to the yield strength in a Dugdale (1960) analysis. The authors concluded that this model does not accurately predict the damage growth with applied compressive load, because the elastic-perfectly plastic constitutive relationship used in the Dugdale model is not an accurate description of material response in the microbuckled region. Independently, the progressive development of damage, leading to ultimate failure

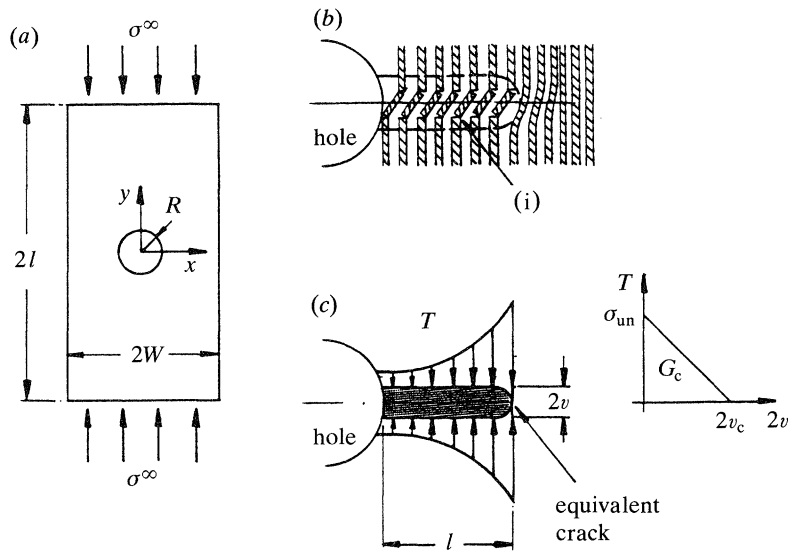

Figure 3. Microbuckled zone at a hole and the equivalent crack used to model the damage zone. (*a*) Schematic of compression-loaded specimen with a hole. (*b*) Microbuckled zone; (i) damage zone (microbuckling and delamination). (*c*) Equivalent crack: normal tractions T, closing displacement $2v$. A linear relation is assumed between T and v. The parameter G_c is the critical value for the energy release rate, and equals the area under the T–$2v$ plot.

has been addressed by Soutis & Fleck (1990) and Soutis *et al.* (1991). A brief description of the latter model is now presented; later the predictions of this model will be compared with the measured notched strength of the T800/924C laminates.

(*a*) *Soutis, Fleck and Smith model for compressive strength*

Consider compressive failure of a finite width, multidirectional composite panel, which contains a central circular hole. It is assumed that microbuckling initiates when the local compressive stress parallel to the 0° fibres at the hole edge equals the unnotched strength of the laminate σ_{un}, that is

$$k_t \sigma^\infty = \sigma_{un}, \tag{3.1}$$

where k_t is the stress concentration factor and σ^∞ is the remote axial stress. Damage development (by microbuckling of the 0° plies, delamination and by plastic deformation in the off-axis plies) is represented by replacing the damage zone by an equivalent crack, loaded on its faces by a crack opening normal traction, T, which decreases linearly with the closing displacement of the crack, $2v$. The crack bridging law is shown schematically in figure 3. It is assumed that the length of the equivalent crack l represents the length of the microbuckle. When the remote load is increased the equivalent crack grows in length, thus representing microbuckle growth. The evolution of microbuckling is determined by requiring that the total stress intensity factor at the tip of the equivalent crack K_{tot} equals zero,

$$K_{tot} = K^\infty + K_T = 0, \tag{3.2}$$

where K^∞ is the stress intensity factor due to the remote stress σ^∞, and K_T is the stress intensity factor due to the local bridging traction T across the faces of the equivalent crack. When this condition is satisfied, stresses remain finite everywhere.

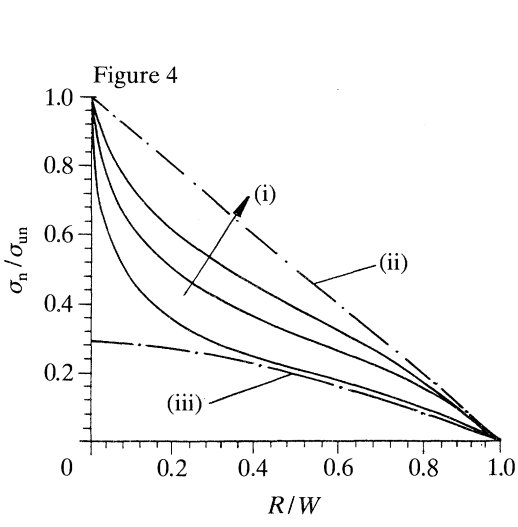

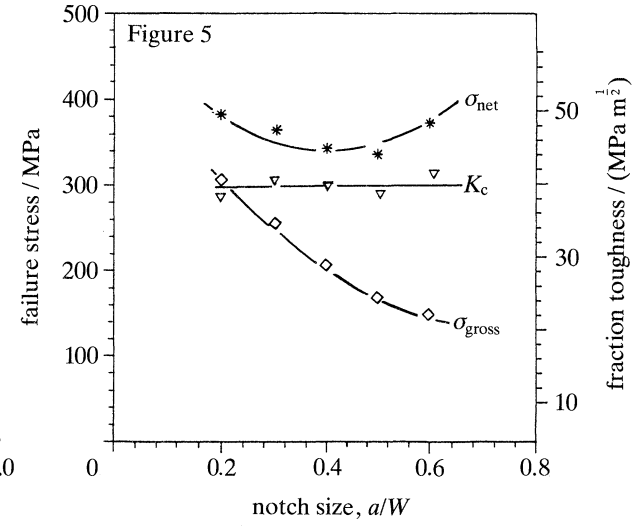

Figure 4. Typical strength predictions of Soutis *et al.* (1991) fracture model, for a plate of width $2W$ containing a central hole of radius R. (i) Increasing $EG_c/\sigma_{un}^2 W$; (ii) $\sigma_n/\sigma_{un} = (1-R/W)$; (ii) $\sigma_n/\sigma_{un} = 1/k_t$.

Figure 5. Compressive failure strength and fracture toughness plotted against (a/W) ratio for a 50 mm wide T800/924C $[(0/90_2/0)_3]_s$ laminate (lay-up L3). ——, Best fit.

The equivalent crack length from the circular hole is deduced as a function of remote stress σ^∞ using the following algorithm. For an assumed length of equivalent crack l, we solve for σ^∞ and for the crack bridging tractions by matching the crack opening profile from the crack bridging law to the crack profile deduced from the elastic solution for a cracked body. The cracked body is subjected to a remote stress σ^∞ and crack face tractions T. At a critical length of equivalent crack, l_{cr}, the remote stress σ^∞ attains a maximum value, designated σ_{cr}, and catastrophic failure occurs.

The model contains two parameters which are measured independently: the unnotched strength σ_{un} and the area G_c under the assumed linear traction–crack displacement curve. σ_{un} is measured from a compression test on the unnotched multidirectional laminate, and G_c is measured from a compressive fracture toughness test. The concept of compressive fracture toughness may be explained as follows. Consider a finite specimen containing a single crack, with a cohesive zone at the crack tip. The cohesive zone is assumed to be much smaller than other in-plane dimensions. Then, stresses decay remotely with radius r from the crack tip as $r^{-\frac{1}{2}}$, characterized by the remote mode I stress intensity factor, K. A cohesive zone exists at the crack tip such that the total stress intensity factor at the tip of the cohesive zone vanishes. Rice (1968) has shown that the work done to advance the crack by unit area G_c equals the area under the crack traction versus crack opening displacement curve,

$$G_c = 2\int_0^{v_c} \sigma(v)\,\mathrm{d}v = \sigma_{un}\, v_c, \tag{3.3}$$

where v_c is the critical crack closing displacement on the crack traction–crack displacement curve, as shown in figure 3. For an orthotropic plate in plane stress, the fracture energy G_c is related to K_c by (Paris & Sih 1969)

$$G_c = (1/2E_{xx}E_{yy})^{\frac{1}{2}}[(E_{xx}/E_{yy})^{\frac{1}{2}} - v_{xy} + E_{xx}/2G_{xy}]^{\frac{1}{2}} K_c^2, \tag{3.4}$$

where E and G are the laminate in-plane extensional and shear moduli, respectively and v is the Poisson's ratio in the reference system shown in figure 3. This is analogous to the fracture mechanics relationship for an isotropic elastic plate in plane stress, $G_c = K_c^2/E$.

We assume that the toughness G_c represents the total energy dissipated by fibre microbuckling, matrix plasticity in the off-axis plies and by delamination. The compressive toughness G_c of a laminate may be measured by preforming a compressive fracture toughness test to measure K_c, and then by using (3.4). The compressive fracture toughness concept is meaningful provided the damage zone at the onset of crack advance is much smaller than other specimen dimensions. Also, the crack faces must not interfere at distances remote from the crack tip. In the next section we report measurements of compressive fracture toughness for T800/924C carbon–epoxy composite.

Predictions of the Soutis *et al.* (1991) are shown schematically in figure 4. The notch strength σ_n decreases with increasing hole radius, R and decreasing toughness G_c.

4. Measurement of compressive fracture toughness

The compressive toughness G_c was determined for laminates L1–L6 of the T800/924C carbon–epoxy material by measuring the compressive fracture toughness G_c of centre cracked specimens. These specimens were 245 mm long by 50 mm wide, and contained central slits perpendicular to the applied load and pre-sharpened by a razor blade. The slits were of sufficient width (about 1 mm) to prevent contact of the slit faces under compressive loading. An antibuckling guide was used to prevent macrobuckling. Tests were performed using a screw driven test machine at a displacement rate of 0.017 mm s^{-1}.

The specimens behaved in an elastic–brittle manner, and the fracture toughness K_c was measured from the failure load. Finite element calculations by the authors confirmed that the K calibration for the centre cracked orthotropic plate is almost identical to that for an isotropic plate, and is given in standard textbooks (see, for example, Paris & Sih 1969; Tada *et al.* 1985).

Typical results are shown in figure 5. For all laminates, the measured fracture toughness K_c is independent of initial notch length, as expected. In contrast, the net section stress and gross section stress at failure are strong functions of notch length. The measured fracture toughness is shown for the six multidirectional laminates in figure 6*a*. The observation that the measured value of K_c is independent of notch length supports the concept of a compressive fracture toughness. No compressive toughness values are reported for the unidirectional material, as failure was by splitting from each end of the notch.

The average fracture toughness is plotted as a function of unnotched compressive strength in figure 6*b*. We note that the measured fracture toughness increases in a roughly linear manner with the measured compressive strength. This suggests that a major contribution to the compressive toughness is from the resistance to failure of the 0° plies.

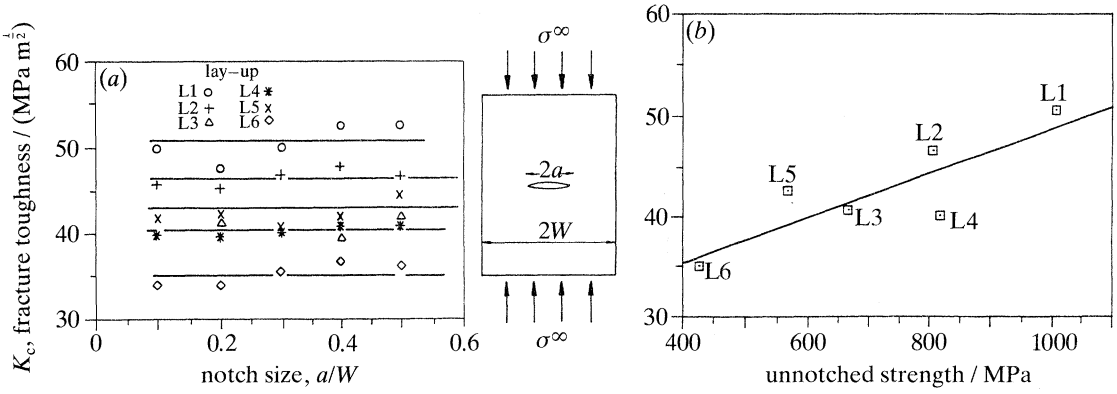

Figure 6. (*a*) Fracture toughness K_c against (a/W) ratio for 50 mm wide T800/924C laminates L1–L6. (*b*) Fracture toughness K_c plotted against unnotched compressive strength for laminates L1–L6. ——, Best fit.

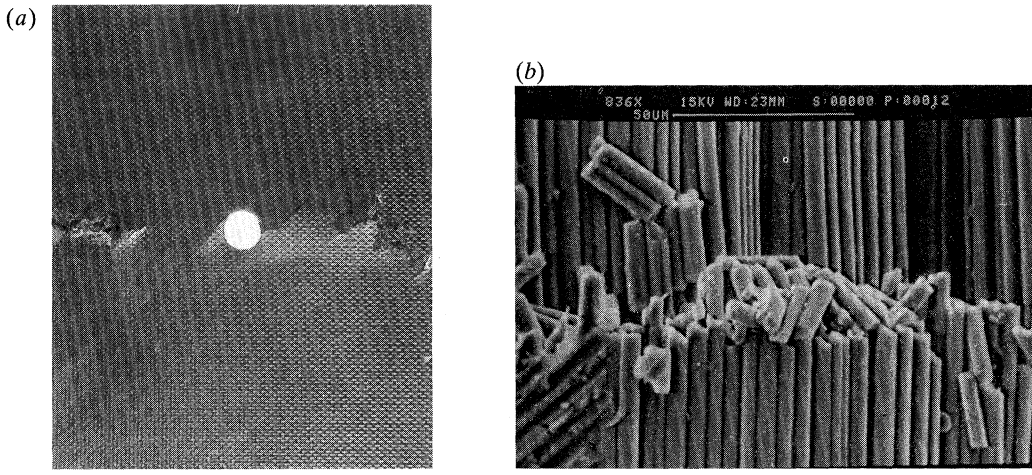

Figure 7. (*a*) Overall failure of a $[(\pm 45/0_2)_3]_s$ laminate showing local delamination, fibre breakage and splitting of the outer 45° plies ($R/W = 0.1$). Hole radius $R = 5$ mm. (*b*) Scanning electron micrographs showing fibre microbuckling in a $[(\pm 45/0_2)_3]_s$ laminate. The buckled zone grows from the edge of the hole in a direction almost perpendicular to the loading axis.

5. Measurement of notched compressive strength

(*a*) *Specimen manufacture*

Specimens of dimensions 245 mm × 50 mm were cut from the 3 mm thick panels of layups L1–L6, and aluminium tabs were bonded onto the ends of the specimens to give a gauge section of 115 mm × 50 mm. Circular holes of diameter 4–25 mm were drilled at the centre of the specimens. Compressive tests were performed by using a screw driven test machine at a displacement rate of 0.017 mm s^{-1}. Load introduction into the specimens was by shear using wedge grips, and an anti-buckling guide was used to prevent macrobuckling of the specimen.

(*b*) *Test results*

All specimens failed from the hole in a direction transverse to the loading axis, as shown in figure 7*a*. The remote failure stress σ_n normalized by the unnotched failure stress σ_{un} of the laminate is shown in figure 8 as a function of hole radius R

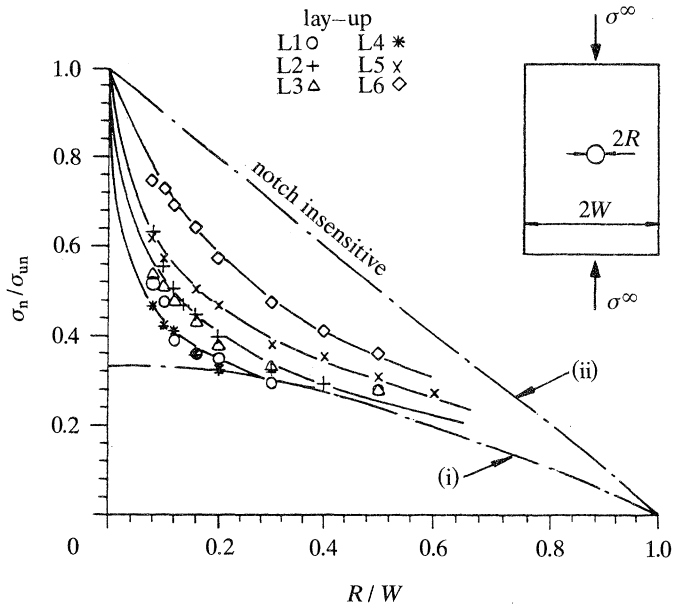

Figure 8. Effect of hole diameter on the compressive strength of T800/924C multidirectional laminates. The stress concentration factor k_t, which defines the notch sensitivity curve, depends upon the degree of orthotropy. The notch sensitive curve (i) shown is for the quasi-isotropic laminate L5; $\sigma_n/\sigma_{un} = 1/k_t$. (ii) $\sigma_n/\sigma_{un} = (1-R/W)$.

normalized by semi-width W of the specimen. In broad terms the failure strength of the notched laminates is approximately half that of the unnotched material. The data for laminates comprising a large proportion of $\pm 45°$ plies lie above that for laminates consisting mainly of 0° plies: the presence of $\pm 45°$ plies reduces the notch sensitivity of the material. This is consistent with the value of the damage parameter $(K_c/\sigma_{un})^2$ for each lay-up, shown in table 1. The damage parameter $(K_c/\sigma_{un})^2$ has the dimensions of length, and gives an approximate measure of the flaw size which the material can tolerate before the failure load becomes dependent upon flaw size. Alternatively, it may be viewed as a measure of the size of the damage zone at failure.

(c) *Development of damage*

Damage development was monitored by using a variety of techniques.

1. The axial strain at various locations on a specimen was measured during a test with the aid of 1 mm × 1 mm strain gauges.

2. X-ray radiography was used upon interruption of several tests. The specimen was removed from the test machine, and zinc iodide solution was applied to improve the discrimination of the X-ray technique. The specimen was then X-rayed.

3. At the end of several tests, the specimen was deplied by burning off the epoxy matrix in an oven, and the individual plies were examined inside a scanning electron microscope.

In all laminates, a damage zone formed at the edge of the hole under increasing remote load. At approximately 75% of the failure load, longitudinal splits occur in the 0° layers at the top and bottom of the hole. These splits degrade the transverse stiffness of the laminate by a small amount, but have a negligible effect upon further damage development and upon the failure load. Microbuckling of the 0° plies nucleates at the sides of the hole at between 75–80% of the failure load, and is

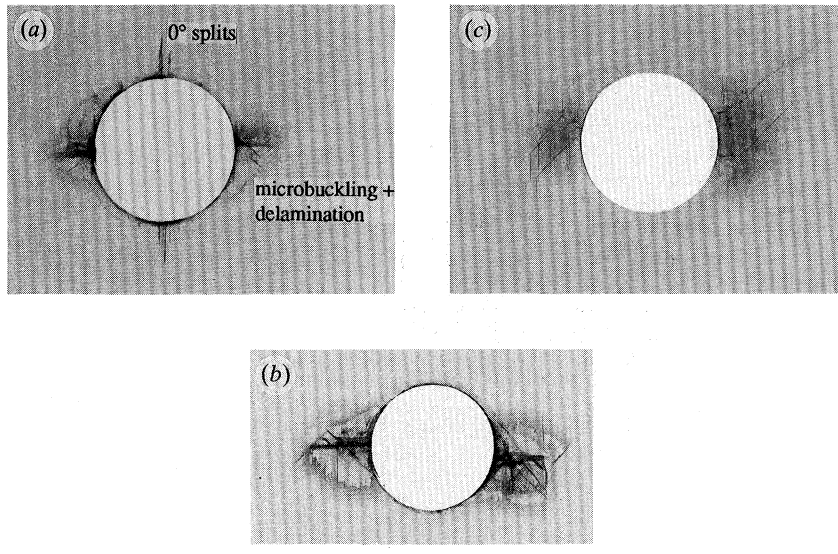

Figure 9. X-ray radiographs showing fibre microbuckling and delamination emanating from a circular hole ($R = 5$ mm) at about 95% of failure load. In all cases the loading direction is from top to bottom. (*a*) $[(\pm 45/0_2)_3]_s$ (L2). (*b*) $[(\pm 45/0/90)_3]_s$ quasi-isotropic laminate (L4). (*c*) $[(\pm 45)_2/0/(\pm 45)_2/0/\pm 45]_s$ (L6).

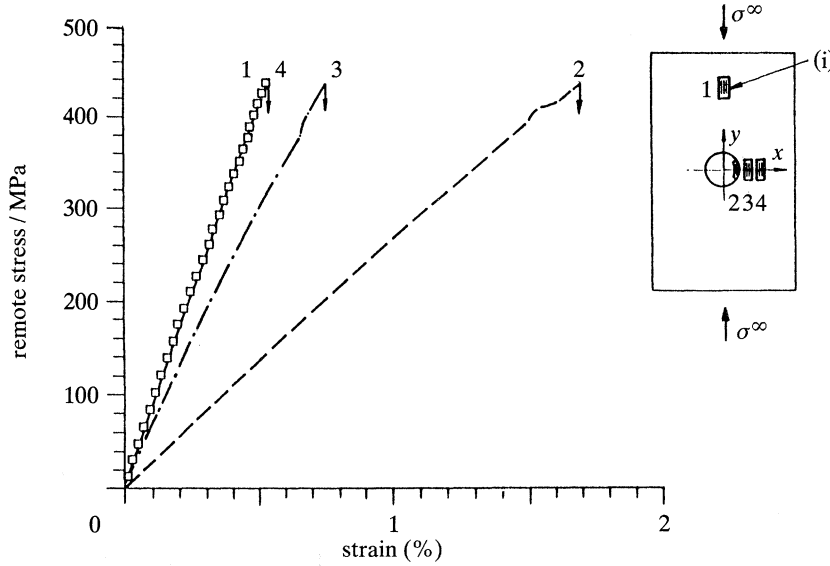

Figure 10. Compressive stress–strain response of a $[(\pm 45/0_2)_3]_s$ notched laminate ($R/W = 0.1$). ——, Average remote strain; – – –, local strain inside hole g_2; —·—, strain at 1 mm from edge of hole g_3; □, strain at 3 mm from edge of hole g_4. (i) Back-to-back strain gauges.

accompanied by matrix cracking of the off-axis plies and delamination between the plies, see figure 9. The damage zone is most extensive in the laminates containing a high proportion of $\pm 45°$ plies. For example, for the $[(\pm 45)_2/0/(\pm 45)_2/0/\pm 45]_s$ laminate L6 and $d = 5$ mm, the delaminated area before failure is 2.8 mm long (x-axis) by 4.8 mm wide (y-axis). For laminates containing a large volume fraction of 0° plies, the damage zone is more crack-like in nature: the damage zone immediately before failure in the $[(\pm 45/0_2)_3]_s$ laminate L2 is 2.6 mm long by 2.0 mm wide.

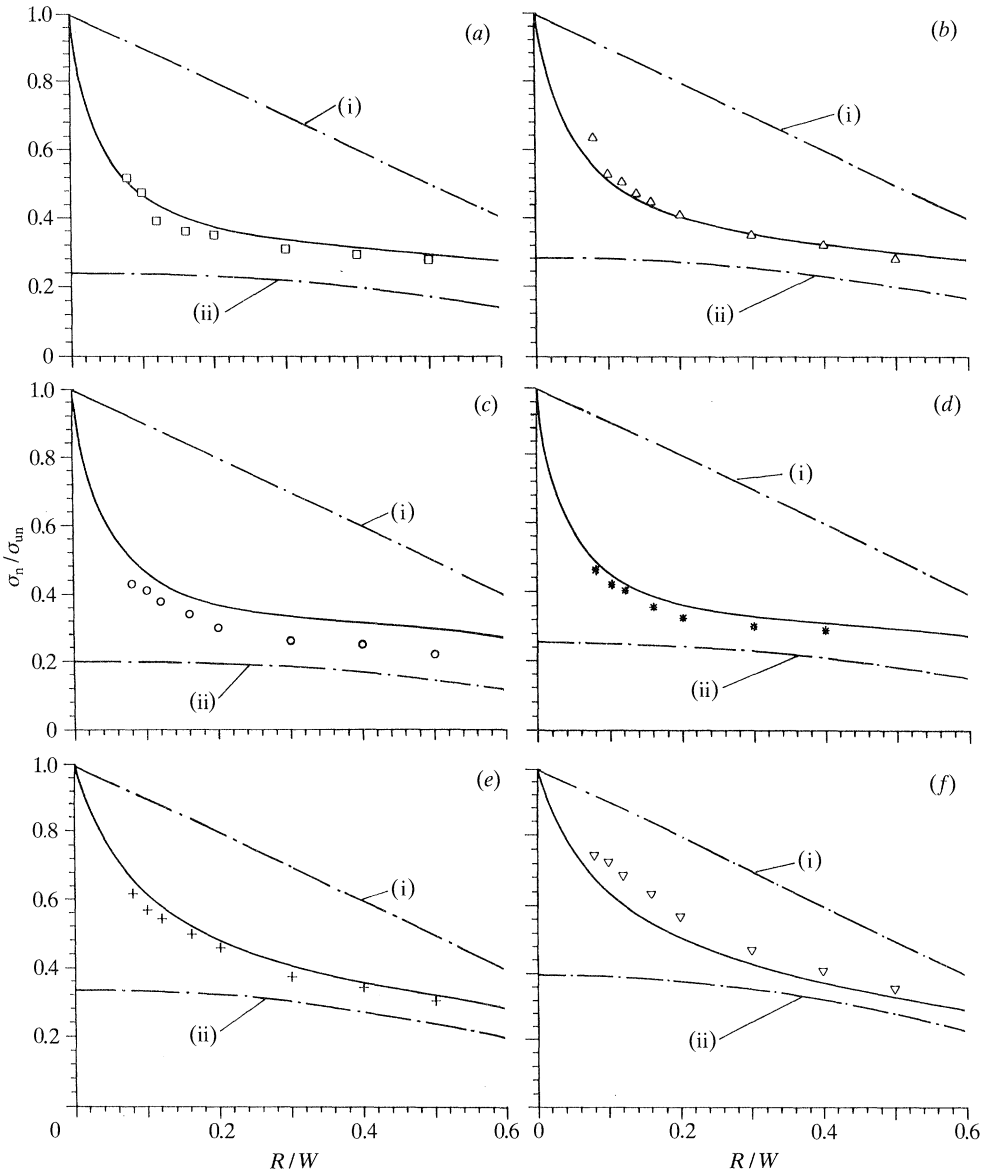

Figure 11. Predictions of compressive strength for 50 mm wide T800/924C laminates for a range of hole diameters. The predictions of the Soutis, *et al.* (1991) model (——) are included. (*a*) □, Laminate L1; (*b*) △, L2; (*c*) ○, L3; (*d*) *, L4; (*e*) +, L5; (*f*) ▽, L6. (i) Net section strength $\sigma_n/\sigma_{un} = 1-R/W$. (ii) $\sigma_n/\sigma_{un} = 1/k_t$.

Microbuckling of the 0° plies from the edge of the hole was apparent by deplying the specimen at the end of a test and by examining the section with a scanning electron microscope, see figure 7*b*. The extent of cracking in the off-axis plies and delamination is limited by the length of the microbuckle zone in the 0° plies.

The stress–strain response for several specimens was determined by placing strain gauges at various locations on the specimens. A typical plot of the response for a $[(\pm 45/0_2)_3]_s$ specimen containing a 5 mm diameter hole is shown in figure 10. Strain gauge 1 was placed remote from the hole. The response for gauges of this type was

linear to failure. Strain gauge 2 (placed inside the hole) and strain gauge 3 (placed adjacent to the edge of the hole) displayed a nonlinear response for loads exceeding approximately 80 % of the failure load. This nonlinearity reflects the development of damage. The local axial strain for the initiation of microbuckling in the notched $[(\pm 45/0_2)_3]_s$ specimen equals 1.5 %, which is 25 % higher than the failure strain of the unnotched specimens. The higher strain for triggering of microbuckling from a hole is believed to be associated with the existence of a strain gradient from the hole: undamaged material surrounds the microbuckled zone and supports it. Under an increasing remote load, the microbuckle zone extends to a length of 2–3 mm, before catastrophic failure occurs.

The $[(0/90_2/0_3]_s$ notched laminate (L3) differed from the other laminates in so far as it had 0° outer plies. Out-of-plane microbuckling initiated at these plies at a local strain level of 1.0 %. In-plane microbuckling developed in the other lay-ups at a local strain level of 1.5 %.

(*d*) *Comparison with theory*

The effect of hole diameter upon failure strength for the laminates L1–L6 is shown in figure 11. The measured notch strengths are bounded by the simple failure criteria of ideally brittle response and the ideally notch insensitive response (Peterson 1974). If the material is ideally brittle, failure occurs when the maximum stress at the hole edge equals the unnotched compressive strength of the material. Alternatively, the ideally notch insensitive material fails when the net section stress equals the unnotched strength. The experimental data for the six lay-ups studied lay between the two limiting behaviours, due to the development of subcritical damage in the form of microbuckling, delamination, matrix plasticity and matrix cracking. The damage reduces the stress concentration at the edge of the hole and delays final failure to higher applied stresses. It should be noted from figure 11 that the angle-play dominated laminate L6 is less notch sensitive than the lay-ups L1–L5 which are dominated by 0° layers. This is consistent with the observation that the extent of subcritical damage is greatest for lay-up L6.

The predictions of the cohesive zone model of Soutis *et al.* (1991) are compared with the measured strength data in figure 11. The model is accurate to within 10 % for the 0° dominated laminates, but is less accurate for laminate L6 which is composed mainly of ±45° plies. For laminate L6 the damage is diffuse in the nature, and a cohesive zone representation of damage becomes inappropriate.

The observed length of the damage zone for the $[(\pm 45/0_2)_3]_s$ laminate (L2) and for the $[(\pm 45)_2/0/(\pm 45)_2/0/\pm 45]_s$ laminate (L6) is shown in figure 12 as a function of the remote load. The observations are made by interrupting a test and using X-ray radiography to monitor the extent of the damage. The predicted development of damage from the Soutis *et al.* (1991) model is included in figure 12. For lay-up L2, it is apparent that the model underestimates the remote stress at which microbuckling initiates but predicts successfully the failure strength and the critical length of the microbuckle. For lay-up L6, the model underestimates the stress for a given microbuckle length by approximately 20 %; the model predicts a critical length of 4.0 mm, compared with an observed length of 2.8 mm. Since laminate L6 contains only 17 % of 0° plies, it is not surprising that the cohesive zone model is inaccurate for this lay-up.

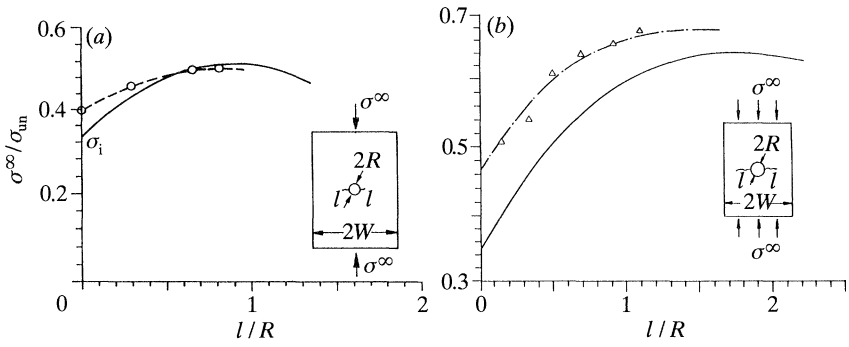

Figure 12. Stable microbuckling growth and failure load for a T800/924C laminate with a 5 mm diameter hole. ——, Theory. (*a*) $[(\pm 45/0_2)_3]_s$, (L2) ——○——; (*b*) $[(\pm 45)_2/0/(\pm 45)_2/0/\pm 45]_s$, (L6), ——△——.

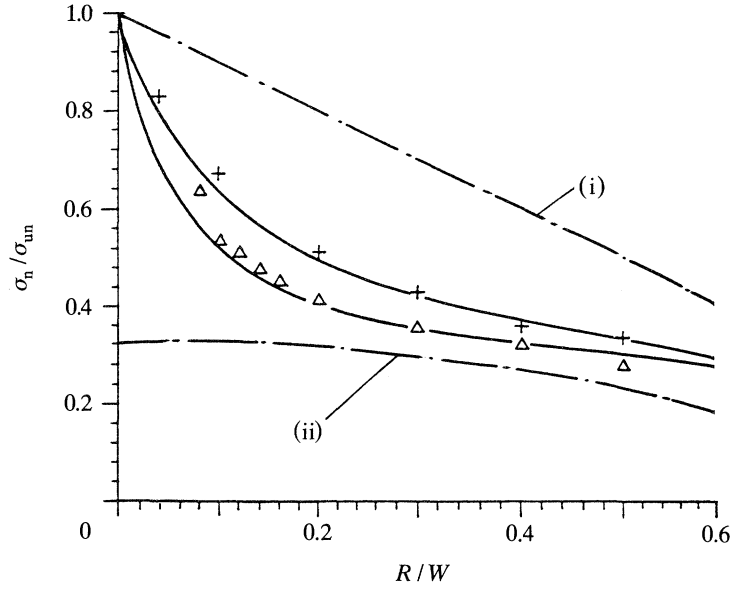

Figure 13. Compressive strength predictions for 50 mm wide $[(\pm 45/0_2)_3]_s$ carbon fibre–epoxy and carbon fibre–PEEK laminates for a range of hole sizes. ——, Theory; △, T800/924C; +, AS4/PEEK. (i) $\sigma_n/\sigma_{un} = 1-R/W$; (ii) $\sigma_n/\sigma_{un} = 1/k_t$.

(*e*) *Effect of matrix upon notched compressive strength*

In other work compressive tests have been performed on AS4 carbon fibres in a PEEK matrix of lay-up L2, $[(\pm 45/0_2)_3]_s$ (Jelf *et al.* 1990). The same specimen geometry was used as in the current study. The AS4 carbon fibres are less strong and stiff than the Toray 800 fibres, and the PEEK thermoplastic material is tougher than the 924C epoxy. The compressive fracture toughness for laminate L2 is 55 MPa $m^{\frac{1}{2}}$ for the AS4/PEEK material compared with 46 MPa $m^{\frac{1}{2}}$ for the T800/924C material.

The notched strength for the AS4/PEEK material is compared with that of the T800/924C material in figure 13. Predictions of the Soutis *et al.* (1991) theory are included in the figure. It should be noted that the AS4/PEEK is less notch sensitive in compression than the T800/924C. The Soutis *et al.* (1991) theory fits the data well, and suggests that the critical microbuckling length is greater for the AS4/PEEK than for the T800/924C composite. Indeed Guynn *et al.* (1989), in their experimental

study of notched compressive strength, observed that the notched ductile system of AS4/PEEK does exhibit a larger critical microbuckle length than the more brittle epoxy matrix systems.

6. Concluding discussion

It has been shown in the present study that the compressive failure of unidirectional and multidirectional unnotched carbon/epoxy composites is controlled by fibre microbuckling. Delamination and plastic deformation in the off-axis plies accompany the microbuckling event. For unnotched specimens, the off-axis plies have only a small influence on the compressive failure strain.

The model of Soutis *et al.* (1991) is able to predict the effects of hole size and lay-up upon the compressive strength and damage zone size at failure. However, this engineering model takes as its input the compressive fracture toughness of the laminate. Further work is required to understand the microstructural origins of the compressive fracture toughness, and to predict it for a multidirectional laminate from lamina or material data.

This work was carried out with the financial support of the Procurement Executive of the Ministry of Defence, and the Science and Engineering Research Council. The authors are grateful for helpful discussions with Professor B. Budiansky of Harvard University and Dr P. A. Smith of Surrey University.

References

Argon, A. S. 1972 *Fracture of composites. Treatise of materials science and technology*, vol. 1. New York: Academic Press.

Awerbuch, J. & Madhukar, M. S. 1985 Notched strength in composite laminates: predictions and experiments – a review. *J. reinforced Plastics Composites* **4**, 3–159.

Budiansky, B. 1983 Micromechanics. *Computers Structures* **16**, 3–12.

Curtis, P. T., Gates, J. & Molneux, C. 1991 An improved engineering test method for the measurement of the compressive strength of unidirectional carbon fibre composites. *RAE Tech. Rep.* 91031.

Curtis, P. T. 1985 *CRAG test methods for the measurement of the engineering properties of fibre reinforced plastics. RAE Tech. Rep.* 85099.

Dugdale, D. S. 1960 Yielding of steel sheets containing slits. *J. Mech. Phys. Solids* **8**, 100–104.

Ewins, P. D. & Ham, A. C. 1973 The nature of compressive failure in unidirectional carbon fibre reinforced plastics. *RAE Tech. Rep.* 73057.

Fleck, N. A. & Budiansky, B. 1992 Compressive failure of fibre composites due to microbuckling. In *Proc. IUTAM Symp. on Inelastic Deformation of Composite Materials* (ed. J. Dvorak), pp. 235–273. Troy, New York, 29 May–1 June 1990.

Guynn, E. G., Bradley, W. L. & Elber, W. 1989 Micromechanics of compression failure in open hole composite laminates. *Composite material: fatigue and fracture* ASTM STP **1012**, 118–136.

Jelf, P. M., Soutis, C. & Fleck, N. A. 1990 Notched compression failure of carbon fibre-PEEK laminates. In *Advanced Composites in Emerging Technologies, 3rd Int. Symposium on Composites, University of Patras, Greece.*

Nuismer, R. J. & Labor, J. D. 1979 Applications of the average stress failure criterion. Part II. Compression. *J. Comp. Mater.* **13**, 49–69.

Paris, P. C. & Sih, G. C. 1969 Stress analysis of cracks. *Fracture toughness applications* ASTM STP **381**, 30–83.

Peterson, R. E. 1974 *Stress concentration factors.* John Wiley.

Rice, J. R. 1968 *Mathematical analysis in the mechanics of fracture* (ed. H. Liebowitz), ch. 3, vol. 2. Academic Press.

Rosen, B. W. 1965 Mechanics of composite strengthening. In *Fiber composite materials*, pp. 37–75. Metals Park, Ohio: American Society of Metals.

Soutis, C. 1991 Measurement of the static compressive strength of carbon fibre-epoxy laminates. *Composites Sci. Technol.* **42**, 373–392.

Soutis, C. & Fleck, N. A. 1990 Static compression failure of carbon fibre T800/924C composite plate with a single hole. *J. Comp. Mater.* **24**, 536–558.

Soutis, C., Fleck, N. A. & Smith, P. A. 1991 Failure prediction technique for compression loaded carbon fibre-epoxy laminate with an open hole. *J. Comp. Mater.* **25**, 1476–1498.

Steif, P. S. 1990*a* A model for kinking in fibre composites. I. Fibre breakage via microbuckling. *Int. J. Solid Structures* **26**, 549–561.

Steif, P. S. 1990*b* A model for kinking in fibre composites. II. Kink band formation. *Int. J. Solid Structures* **26**, 563–569.

Tada, H., Paris, P. C. & Irwin, G. 1985 *The stress analysis of cracks handbook*, 2nd edn. St Louis, Missouri: Paris Productions.

Whitney, J. M. & Nuismer, R. J. 1974 Stress fracture criteria for laminated composites containing stress concentrations. *J. Comp. Mater.* **8**, 253–265.

Yurgatis, S. W. 1987 Measurement of small angle misalignments in continuous fibre composites. *Composites Sci. Technol.* **30**, 279–293.

Received 21 November 1991; accepted 23 September 1992